

Parametric Estimation of the Orientation of Textured Planar Surfaces

Joseph M. Francos, *Senior Member, IEEE*, and Haim H. Permuter

Abstract—This paper presents a parametric solution to the problem of estimating the orientation in space of a planar textured surface, from a single, noisy, observed image of it. The coordinate transformation from surface to image coordinates, due to the perspective projection, transforms each homogeneous sinusoidal component of the surface texture into a sinusoid whose frequency is a function of location. The functional dependence of the sinusoid phase in location is uniquely determined by the tilt and slant angles of the surface. Using the phase differencing algorithm we fit a polynomial phase model to a sinusoidal component of the observed texture. Assuming the estimated polynomial coefficients are the coefficients of a Taylor series expansion of the phase, we establish a linear recursive relation between the model parameters and the unknown slant and tilt. A linear least squares solution of the resulting system provides the slant and tilt estimates. To improve accuracy, an iterative refinement procedure is applied in a small neighborhood of these estimates. The performance of the proposed algorithms is evaluated by applying them to images of different planar surfaces, and by comparing their statistical performance with the Cramer–Rao bound. The combined two-stage algorithm is shown to produce estimates that are close to the bound.

Index Terms—Nonhomogeneous two-dimensional signals, parametric texture modeling, perspective estimation, two-dimensional polynomial phase models.

I. INTRODUCTION

THE perspective projection has a dominant and fundamental role in any imaging process, whether by the human visual system, or by some type of a camera. Hence, perspective is one of the prominent clues in image interpretation and understanding. This makes perspective estimation a key problem in many image modeling and analysis applications. A closely related problem is the estimation of the shape of a three-dimensional (3-D) rigid body from one, or more, images of that body. One of the possible approaches toward a solution of this problem is known as “shape from texture,” where estimation of the shape of the rigid body is based on its surface texture information. In general, recovery of 3-D shape from texture is possible if some prior knowledge about the surface texture, in the surface coordinate system, is available. Due to

the perspective projection the observed texture has properties different from those of the surface texture. Thus, 3-D shape information can be computed such that the discrepancy is accounted for. For example, if the true texture is known to be an array of elements with a known shape, say circular, the surface gradient can be inferred from the observed distorted shape, elliptical in this case, of the elements. In this paper we address a special case of the general problem of estimating shape from texture: We consider the problem of estimating the orientation in space of a planar textured surface, from a single, noisy, observed image of it.

A solution to this problem is an essential component in many image processing and multimedia data processing applications. For example, the segmentation of two-dimensional (2-D) or 3-D images and video for content-based coding and representation is considerably simplified if the effects of the perspective projection are eliminated first, thus reducing the nonhomogeneity of the image. By estimating and then canceling the effect of the perspective projection on a given image, we avoid the difficulty of segmenting and coding an image where each of its patches is nonhomogeneous. Furthermore, to enable content-based indexing for retrieval from multimedia data bases, the effect of the specific perspective projection in each image has to be nulled in order to “normalize” all images with respect to some “common basis.” In particular, in indexing and retrieval systems of multimedia data that employ the textural information in the imagery components of the data, e.g., [12], the identification of similar textured surfaces as being such, is impossible unless the effects of the different perspective projections involved in the process of taking each of the images are estimated and then removed. We therefore conclude that all the foregoing applications require an accurate estimate of the perspective transformation to become available at a moderate computational complexity, so that perspective estimation could be conveniently integrated into the higher level applications.

Existing solutions to problems where perspective estimation is involved attempt to extract the projection parameters based on the observed variations in the image, generated by the perspective projection. The structure-based approaches attempt to recognize the structure of the surface texture (the “true” texture) from the observed projected image of that surface. In other words, in order to estimate the projection parameters, these methods must first (or jointly with estimating the projection parameters as proposed by [5]) obtain the characterizing properties of the surface texture such as regularity, periodicity, symmetry, collinearity, etc. (see, e.g., [6] and the references therein). This task is very difficult in general, and more so in the presence of noise, since due to the projection distortion and

Manuscript received November 19, 1998; revised August 18, 2000. This work was supported in part by the Israel Ministry of Science, Eshkol Fellowship Program in Applied Mathematics under Grant 0616196, in part by the Israel Ministry of Science and the French Ministry of Research and Technology under Grant 8814196, and in part by the Israel Ministry of Science under Grant 8635297. The associate editor coordinating the review of this manuscript and approving it for publication was Prof. Patrick Bouthemy.

J. M. Francos and H. Permuter are with the Department of Electrical and Computer Engineering, Ben-Gurion University, Beer-Sheva 84105, Israel (e-mail: francos@ee.bgu.ac.il).

Publisher Item Identifier S 1057-7149(01)00614-5.

the noise contribution the observed surface does not exhibit the expected “regularities,” and texture elements (“texels”) are difficult to identify [5]. An alternative approach, that does not require the initial recognition of the structure of the surface texture is based on statistical assumptions regarding the distribution of textural properties of the surface texture. Typical assumptions are isotropy, [1], [2], [8], [13] and homogeneity, [3], [6], [14]. Thus, an observed preferred orientation of an isotropic surface texture, or an observed inhomogeneity of a homogeneous surface texture, is employed to estimate the surface orientation. We note that many of the foregoing methods (see, e.g., [6], [11], [3], [4]) are derived for binary images, or are based on an initial local analysis of the image, using its edge information. Hence, their usefulness in the presence of noise is limited.

In [5] a two-step procedure for texel identification and surface estimation is proposed. An *ad-hoc* procedure based on a multiscale region detector and some simplifying assumptions is used to construct a set of candidate texels. In a second stage, perspective viewing constraints are employed to select the true texels from the candidates, while simultaneously constructing an approximation of the surface orientation. The algorithm proposed in [14] evaluates the dominant frequency at each image point using the wavelet transform, and then employs the spatial dependence of this frequency component to estimate the surface orientation. A different method for estimating and canceling, the effects of perspective based on the 1-D Chirplet transform was suggested in [15]. More recently, an algorithm for estimating the surface orientation by first evaluating the ridge surface of a continuous wavelet transform of the observed textured image was derived in [17]. This approach employs the fact that the dominant spatial frequencies of a textured image are characterized by ridge points of the wavelet transform, to evaluate the surface tilt and slant angles from the parameters of these ridge points.

Generally speaking, these algorithms address the problem of estimating the *instantaneous frequency* at every image point (or a related quantity) as a first step in a procedure for estimating the tilt and slant of the observed surface, based on the variations of the instantaneous frequency. This approach is further pursued with the introduction of novel space-frequency methods, see e.g., [14], [7]. However, given a nonhomogeneous signal $d(x_i, y_i)$, the question of the unique determination of its instantaneous phase, frequency and amplitude, is not a straight forward one, as even in the one dimensional case incoherent definitions of instantaneous phase and amplitude are common. We refer the interested reader to [22] for a detailed discussion on the one-dimensional problem. Following, [22] it is clear that starting from a given signal $d(x_i, y_i)$, it is possible to introduce an infinite number of pairs $[a(x_i, y_i), \Phi(x_i, y_i)]$ such that

$$d(x_i, y_i) = a(x_i, y_i) \cos(\Phi(x_i, y_i)), \quad (1)$$

Nevertheless, in order to be able to interpret $a(x_i, y_i)$ as the instantaneous amplitude of the signal, and $\Phi(x_i, y_i)$ as its instantaneous phase, the instantaneous phase and amplitude should be defined in such a way that only a *single*, well defined, pair $[a(x_i, y_i), \Phi(x_i, y_i)]$ will correspond to any given signal $d(x_i, y_i)$, so that the representation (1) is unique. We shall further elaborate on this point in Section IV.

A maximum likelihood estimator for the tilt and slant parameters is proposed in [9]. In this framework the homogeneous surface texture is modeled by a Gauss–Markov random field. A probability distribution function for the observed textured image, assuming a “linear” projection model (instead of the nonlinear perspective projection transformation) is derived. The joint problem of estimating the surface orientation parameters, and the texture model is then solved by a ML estimator. However, due to the linear approximation of the projection transformation, the method was found to be sensitive to the nonhomogeneities of the observed texture which are especially significant for low slant angles.

In this paper we elaborate on the problem of estimating the orientation in space of a planar textured surface from a single, noisy, observed image of it, such that, in its own coordinate system the surface texture is *homogeneous*. By employing a general texture model which is based on the 2-D Wold-like decomposition of homogeneous random fields, and substituting the physical model of the perspective projection, we derive an accurate and physically meaningful model for the observed image of the planar surface. Using the derived model of the observed nonhomogeneous image, two algorithms are rigorously developed. The performance of the proposed algorithms is evaluated through Monte-Carlo simulations. The error variance in estimating the tilt and slant parameters in the presence of noise is compared with the Cramer–Rao bound for this problem, derived in [29]. To the best of our knowledge the derivation of estimation algorithms in the presence of noise, and the evaluation of their performance relative to a universal performance bound, were never considered in the existing literature. Furthermore, since the model of the homogeneous surface texture is based on the 2-D Wold decomposition of homogeneous random fields, the proposed algorithms provide a unifying framework for both the structural and statistical methods. In addition, the extremely difficult task of identifying the texture elements from the perspective projected noisy image, as required by the structure-based approaches, is avoided.

More specifically, the 2-D Wold decomposition implies that the deterministic component of any homogeneous texture field can be approximated by a sum of 2-D sinusoids, [23]. Thus, an approximate model of the surface texture deterministic component is given by

$$t(x_s, y_s) = \sum_{l=1}^L A_l \cos(x_s \omega_l + y_s \nu_l + \varphi_l) \quad (2)$$

where (x_s, y_s) denote the surface coordinates. The coordinate transformation from surface to image coordinates, due to the perspective projection, transforms each homogeneous sinusoidal component to a sinusoid whose frequency is a function of location. In the Appendix it is proved that in the case of a planar surface, the functional dependence of the sinusoid phase in location is uniquely determined by the tilt and slant angles of the surface. Hence, the surface tilt and slant angles can be recovered from the phase of the sinusoidal component, measured in the image plane.

The perspective projection results in a continuous coordinate transformation from the surface coordinate system to the

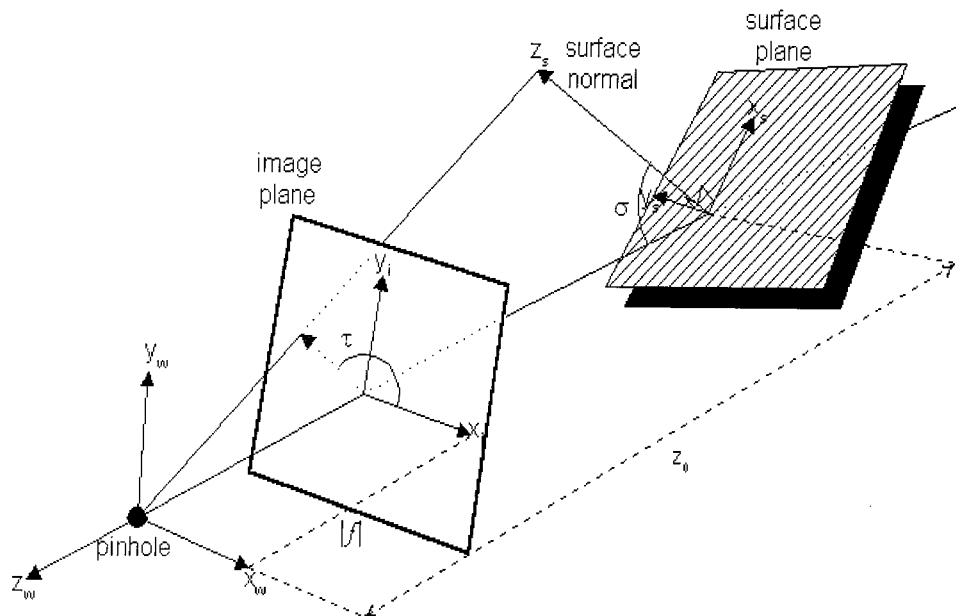


Fig. 1. Perspective projection.

image coordinate system. Hence, the phase function of each sinusoidal component of the surface texture is transformed by the perspective projection into a nonlinear, continuous function of the image coordinates. Since continuous functions can be approximated by polynomials, a natural choice for modeling the continuous phase function of each sinusoidal component is by a polynomial function of the image coordinates. Hence, the model of the harmonic component of a homogeneous surface texture projected onto the image plane by the perspective projection is a multicomponent model, where each component is of a constant amplitude times a sine of a polynomial function of the image coordinates.

The paper is organized as follows. In Section II we present the viewing geometry we use and the resulting functional dependence of the observed phase on the image coordinates, for each sinusoidal component of the surface texture. In Section III we briefly present the polynomial phase model and a corresponding algorithm for estimating its parameters. However, this estimation algorithm is designed to work with complex valued constant amplitude polynomial phase monocomponent signals. In our application the 2-D signal is real, and in general it has more than a single component. Therefore, in Section IV we derive an algorithm that isolates a single component from the observed signal and converts it into a complex form through the 2-D Hilbert transform, such that the concepts of 2-D instantaneous phase, frequency, and amplitude are well defined. In Section V we derive a computationally efficient algorithm for estimating the slant and the tilt of the planar surface directly from the estimated polynomial model of the phase. In order to do so it is assumed that the estimated polynomial phase coefficients are in fact, the coefficients of a Taylor series expansion of the phase. In Section VI we present an iterative algorithm to improve the accuracy of the obtained tilt and slant estimates. In Section VII we illustrate the performance of the proposed algorithms using synthetic and photographed images. In particular, we investigate the performance of the algorithms in the presence

of noise and analyze their performance through Monte-Carlo simulations and by comparing the Monte-Carlo results with the Cramer–Rao lower bound (CRLB). Finally, in Section VIII we make some concluding remarks.

II. THE PERSPECTIVE TRANSFORMATION

This section defines the viewing geometry we use. In the following we adopt the notations used by Super and Bovik in [14] and assume a pinhole perspective projection model, since it provides a good approximation to a lens-type imaging system.

Assign a world coordinate system $\mathbf{x}_w = [x_w \ y_w \ z_w]^T$ to the imaging system such that its origin is at the focal point and the $-z_w$ axis is the optical axis (see Fig. 1). The image plane is located at $z_w = f < 0$ where $|f|$ is the focal length. Define the image plane coordinate system $\mathbf{x}_i = [x_i \ y_i]^T$ such that $x_i = x_w$ and $y_i = y_w$.

We use the slant-tilt system for representing the orientation of the planar surface. The slant, σ , is the angle between the surface normal and the optical axis z_w . The tilt, τ , is the angle between the x_i -axis and the projection of the surface normal onto the image plane. To describe a texture on the surface, we must define a coordinate system $\tilde{\mathbf{x}}_s = [x_s \ y_s \ z_s]^T$ on the surface. This coordinate system is formed by

- 1) setting the z_s -axis to be the surface normal;
- 2) setting the x_s -axis to be the back-projection onto the surface of the image tilt vector $(\cos \tau, \sin \tau)$;
- 3) setting the y_s -axis so as to form right-handed orthogonal coordinate system;
- 4) setting the origin at the intersection of the surface with the z_w -axis.

Thus, the coordinate transformation from the surface coordinate system to the world coordinate system is given by

$$\mathbf{x}_w = \begin{bmatrix} \cos \sigma \cos \tau & -\sin \tau & \sin \sigma \cos \tau \\ \cos \sigma \sin \tau & \cos \tau & \sin \sigma \sin \tau \\ -\sin \sigma & 0 & \cos \sigma \end{bmatrix} \tilde{\mathbf{x}}_s + \begin{bmatrix} 0 \\ 0 \\ z_0 \end{bmatrix} \quad (3)$$

where z_0 is the z_w -coordinate of the surface where it crosses the optical axis.

The coordinate transformation of a point in the world coordinate system to image coordinates due to the perspective projection is given by

$$\mathbf{x}_i = \frac{f}{z_w} \begin{bmatrix} 1 & 0 & 0 \\ 0 & 1 & 0 \end{bmatrix} \mathbf{x}_w. \quad (4)$$

Since for any surface point we have by definition that $z_s = 0$, let us define $\mathbf{x}_s = [x_s \ y_s]^T$ to be the coordinate vector of a surface point. Therefore, the surface to world coordinate transformation of a point *on* the surface is given using (3) by

$$\mathbf{x}_w = \begin{bmatrix} \cos \sigma \cos \tau & -\sin \tau \\ \cos \sigma \sin \tau & \cos \tau \\ -\sin \sigma & 0 \end{bmatrix} \mathbf{x}_s + \begin{bmatrix} 0 \\ 0 \\ z_0 \end{bmatrix}. \quad (5)$$

For any point of the surface we have that its z_w coordinate is given by

$$z_w = z_0 - x_s \sin \sigma. \quad (6)$$

Substituting (5) and (6) into (4) we obtain the surface to image coordinate transformation of a point *on* the surface to a point on the image plane due to the perspective projection

$$\frac{\mathbf{x}_i}{f} = \frac{1}{z_0 - x_s \sin \sigma} \begin{bmatrix} \cos \tau & -\sin \tau \\ \sin \tau & \cos \tau \end{bmatrix} \begin{bmatrix} \cos \sigma & 0 \\ 0 & 1 \end{bmatrix} \mathbf{x}_s. \quad (7)$$

The matrix $\begin{bmatrix} \cos \tau & -\sin \tau \\ \sin \tau & \cos \tau \end{bmatrix}$ is a rotation matrix, and the matrix $\begin{bmatrix} \cos \sigma & 0 \\ 0 & 1 \end{bmatrix}$ provides the projection of \mathbf{x}_s to \mathbf{x}_i/f for a zero tilt. The term $1/(z_0 - x_s \sin \sigma)$ is a scaling factor due to the distance of the surface from the pinhole.

The inverse of the relation (7) is given by

$$\mathbf{x}_s = z_w \begin{bmatrix} \sec \sigma & 0 \\ 0 & 1 \end{bmatrix} \begin{bmatrix} \cos \tau & \sin \tau \\ -\sin \tau & \cos \tau \end{bmatrix} \frac{\mathbf{x}_i}{f} \quad (8)$$

where substitution of (8) into (6) yields

$$z_w = \frac{z_0}{\tan \sigma \left(\frac{x_i}{f} \cos \tau + \frac{y_i}{f} \sin \tau \right) + 1}. \quad (9)$$

A. Projection of the Texture

Next, we derive a model for the harmonic component of a texture field, undergoing a perspective projection.

Substituting the inverse coordinate transformation expression (8) into the texture model (2), we obtain the model of the harmonic component, projected onto the image plane, i.e.,

$$t_i(\mathbf{x}_i) = t_s[\mathbf{x}_s(\mathbf{x}_i)] = \sum_{l=1}^L A_l \cos(\Phi_l(\mathbf{x}_i)) \quad (10)$$

where $\Phi_l(x_s, y_s) = x_s \omega_l + y_s \nu_l + \varphi_l$ is given in the image coordinate system by

$$\begin{aligned} & \Phi_l(x_i, y_i) \\ &= \frac{x_i (\tilde{u}_l \cos \tau - \tilde{v}_l \cos \sigma \sin \tau)}{f \cos \sigma} + \frac{y_i (\tilde{u}_l \sin \tau + \tilde{v}_l \cos \sigma \cos \tau)}{f \cos \sigma} \\ & \quad \frac{1}{\tan \sigma \left(\frac{x_i}{f} \cos \tau + \frac{y_i}{f} \sin \tau \right) + 1} \\ & \quad + \varphi_l \end{aligned} \quad (11)$$

and

$$\tilde{u}_l = \omega_l z_0$$

$$\tilde{v}_l = \nu_l z_0.$$

Following the definition in the 1-D case, we call real 2-D signals with constant instantaneous amplitude, *2-D phase signals*.

Since the origin of the observed surface is projected onto the origin of the image, we conclude that for each harmonic component of the surface texture, its projection on the image has the same initial phase φ_l as on the surface. This is because the initial value of each cosine function, i.e., its value at $(0, 0)$, remains unchanged under a projection that keeps the origin.

III. THE PARAMETRIC PHASE MODEL AND ITS ESTIMATION

In the previous section it is concluded that the phase function of any sinusoidal component of the homogeneous surface texture is transformed by the perspective projection into a non-linear function of the image coordinates. As shown in the Appendix, for a given focal length, the transformation is a unique function of the surface tilt and slant angles. Hence, in principle, the surface tilt and slant can be recovered from the phase of the projected sinusoidal component, measured on the image plane. However, due to its 2π periodicity the phase wraps around, and only its principle value is observable. Therefore, any use of the phase information is limited by the need to first unwrap the phase of the observed signal.

In this paper we propose to use a parametric model as an alternative to the need to employ phase unwrapping methods. (For an overview of 2-D phase unwrapping algorithms, see, e.g., [24] and the references therein.) Since continuous functions can be approximated by polynomials, a natural choice for modeling any *continuous* 2-D phase function is by a 2-D polynomial of the coordinates. Since the assumption of phase smoothness is implicit to this model, no *explicit* phase unwrapping is required in estimating the observed phase.

In this section we briefly study the model of a single component, constant amplitude exponential of a polynomial function of the field coordinates. This model belongs to the general class of AM-FM signals, [25], [26]. The model, as well as the properties of the parametric phase estimation algorithm, described in this section, are studied in detail in [18] and [19]. More specifically, let $\{v(x, y)\}$ be a discrete 2-D constant amplitude polynomial phase signal, i.e.,

$$v(x, y) = A \exp\{j\phi_{Q+1}(x, y)\}, \quad \begin{aligned} x &= 0, 1, \dots, N-1, \\ y &= 0, 1, \dots, M-1 \end{aligned} \quad (12)$$

where

$$\phi_{Q+1}(x, y) = \sum_{\{0 \leq k, \ell; 0 \leq k+\ell \leq Q+1\}} c(k, \ell) x^k y^\ell. \quad (13)$$

We call $\phi_{Q+1}(x, y)$ 2-D polynomial of *total-degree* $Q+1$. The amplitude A is a real valued positive constant. To simplify the presentation we assume there is no observation noise and $A \equiv 1$. Hence, $v(x, y) = \exp\{j\phi_{Q+1}(x, y)\}$.

The proposed phase estimation algorithm is suboptimal (relative to the maximum likelihood estimator), but computationally efficient (since no multidimensional search in the parameter

space is required). The algorithm is based on the properties of a 2-D phase difference operator. First we give a brief heuristic explanation of the idea behind the operator.

Consider the observed signal which is given by (12), and assume for the moment that x and y are continuous variables. By differentiating the phase of the observed signal P times along the x axis and $Q - P$ times along the y axis, (in any order, as long as the total number of differentiation operations in both axes is Q), we obtain a 2-D complex exponential signal. It can be shown that the spatial frequency (ω, ν) of this complex exponential is a function of two of the coefficients of the highest “layer,” $Q+1$, of the phase polynomial, and other known quantities. The exact functional relation of the exponential spatial frequency and the phase parameters is given later in this section. By estimating the frequency of the complex exponential we obtain estimates of two of the coefficients of the highest “layer” of the phase polynomial model. Repeating this procedure for all $0 \leq P \leq Q$, all the coefficients of the highest “layer,” $Q + 1$, of the phase polynomial model are estimated.

Having completed the estimation of the phase parameters in the highest “layer,” their contribution to the signal phase can be eliminated, thus resulting in a polynomial phase signal of total-degree Q . By repeating this entire process for all the “layers” in the phase model, all the phase parameters are estimated.

Since in our problem the variables x and y are discrete, phase differentiating will be replaced by phase differencing. In principle, this could be accomplished by computing the phase of the 2-D signal and then performing the differencing operation. However, extraction of the phase function is difficult, and especially in the presence of noise, because of the need to perform phase unwrapping. As we will show next, phase differencing can be accomplished *without* phase unwrapping, by performing a certain nonlinear operation on the 2-D signal, using what we call “the phase differencing (PD) operator.” We next define the basic polynomial phase differencing operators.

Definition 1: Let τ_y and τ_x be some positive constants. Define

$$\begin{aligned} \text{PD}_{y(0)}[v(x, y)] &= v(x, y) & x = 0, 1, \dots, N-1, \\ & & y = 0, 1, \dots, M-1 \end{aligned} \quad (14)$$

and in general

$$\begin{aligned} \text{PD}_{y(q)}[v(x, y)] \\ = \text{PD}_{y(q-1)}[v(x, y)] (\text{PD}_{y(q-1)}[v(x, y + \tau_y)])^* \end{aligned} \quad (15)$$

where the resulting 2-D signal $\text{PD}_{y(q)}[v(x, y)]$ exists for $x = 0, 1, \dots, N-1, y = 0, 1, \dots, M-1 - q\tau_y$. The phase differencing operator along the x -axis, $\text{PD}_{x(P)}[v(x, y)]$ is defined in a similar way.

Assume we have sequentially applied the phase difference operator $\text{PD}_{x(P)}$ P times, and the phase difference operator $\text{PD}_{y(Q-P)}$ $Q - P$ times, to some complex-valued 2-D signal $v(x, y)$. We will denote the resulting signal by $\text{PD}_{x(P), y(Q-P)}[v(x, y)]$.

Theorem 1: Let $v(x, y)$ be given by (12) and (13). Then, the signal $\text{PD}_{x(P), y(Q-P)}[v(x, y)]$ is a 2-D exponential given by

$$\begin{aligned} \text{PD}_{x(P), y(Q-P)}[v(x, y)] \\ = \exp\{j[\omega_Q x + \nu_Q y + \gamma_Q(\tau_x, \tau_y)]\}, \\ x = 0, 1, \dots, N-1 - P\tau_x, \\ y = 0, 1, \dots, M-1 - (Q-P)\tau_y \end{aligned} \quad (16)$$

where

$$\omega_Q = (-1)^Q c(P+1, Q-P)(P+1)!(Q-P)! \tau_x^P \tau_y^{Q-P}, \quad (17)$$

$$\nu_Q = (-1)^Q c(P, Q+1-P)P!(Q+1-P)! \tau_x^P \tau_y^{Q-P} \quad (18)$$

and $\gamma_Q(\tau_x, \tau_y)$ is not a function of x nor y .

Theorem 1 implies that applying in some arbitrary sequence, P times the operator $\text{PD}_{x(1)}$, and $Q - P$ times the operator $\text{PD}_{y(1)}$, to the observed signal (12), the resulting signal is the 2-D exponential $\text{PD}_{x(P), y(Q-P)}[v(x, y)] = \exp\{j[\omega_Q x + \nu_Q y + \gamma_Q(\tau_x, \tau_y)]\}$ where ω_Q and ν_Q are given by (17) and (18), respectively. We can thus reduce any 2-D nonhomogeneous, polynomial phase signal, $v(x, y)$, whose phase is of total-degree $Q + 1$, to a 2-D single tone signal whose frequency is (ω_Q, ν_Q) .

Hence, estimating (ω_Q, ν_Q) using any standard frequency estimation technique, results in an estimate of $c(P+1, Q-P)$, and $c(P, Q+1-P)$. In this paper we estimate the frequency of the exponential using a search for the maximum of the absolute value of the signal 2-D Discrete Fourier Transform (2-D DFT). Repeating the procedure which was described above assuming some arbitrary P , for all P such that $0 \leq P \leq Q$, we obtain estimates of all the parameters of the highest order layer, $Q + 1$ of the phase model. Multiplying $v(x, y)$ by $\exp\{-j \sum_{k=0}^{Q+1} \hat{c}(k, Q+1-k)y^{Q+1-k}x^k\}$ results in a new polynomial phase signal whose total-degree is Q . By applying to the resulting signal a procedure similar to the one used to estimate the parameters $c(k, \ell)$ for $k + \ell = Q + 1$, we obtain an estimate of the $Q + 1$ parameters in the Q “layer.”

In general, let $v^{(q+1)}(x, y)$ denote the 2-D signal, where $q+1$ denotes the *current* total-degree of its phase polynomial. By repeating for all $q = Q, \dots, 0$, the two basic steps of estimating the $c(k, \ell)$ parameters of “layer” $q + 1$ through finding the maxima of

$$\left| \text{DFT} \left(\text{PD}_{y(q-P)} \left[\text{PD}_{x(P)} \left[v^{(q+1)}(x, y) \right] \right] \right) \right|$$

for all $0 \leq P \leq q$, followed by multiplying the already reduced order 2-D polynomial phase signal by $\exp\{-j \sum_{k=0}^{q+1} \hat{c}(k, q+1-k)y^{q+1-k}x^k\}$ in the next step, we obtain estimates for all the phase parameters except $c(0, 0)$. The resulting signal after this processing, $v^{(0)}(x, y)$, is a constant phase 2-D signal. Taking now the average of the imaginary part of the logarithm of this signal we obtain an estimate for $c(0, 0)$. We have thus completed the estimation of all the coefficients of the 2-D phase polynomial of total-degree $Q+1$. In the following we refer to the algorithm as the *phase differencing algorithm* (PD algorithm).

So far we described the parameter estimation algorithm for the case in which no observation noise exists. However, in many practical situations the signal is observed in the presence of additive noise. Thus, a straightforward but computationally prohibitive alternative to the PD Algorithm is to develop a maximum likelihood estimator for the polynomial phase parameters. This estimator involves a multidimensional search in the parameter space and is not practical except for very low order models. It turns out, [18] that although the PD algorithm is suboptimal (relative to the ML algorithm), its performance in the presence of additive white noise, is close to the Cramer–Rao lower bound (CRLB) on the error variance in estimating the parameters of the polynomial phase model, for moderate to high signal to noise ratios.

IV. EXTRACTION OF A MONOCOMPONENT COMPLEX VALUED SIGNAL

As already indicated in Section I, most of the existing algorithms attempt to estimate the *instantaneous frequency* at every image point (or some related quantity) and to estimate the tilt and slant of the observed surface by analyzing the variations of the instantaneous frequency, e.g., [7], [10], [14], [15], [17]. However, it seems that the problem of how to rigorously define the instantaneous frequency of a 2-D nonhomogeneous signal is overlooked. Hence, there is no guarantee that the instantaneous frequency is being correctly estimated.

Starting from the physical model of the observed nonhomogeneous signal (10), (11), one would like to obtain a coherent definition of the instantaneous frequency of the signal, or of its individual components. Yet, to keep the physical interpretation of the model meaningful, it is clear from (10) that we would like the instantaneous amplitude of each component to be a constant. Let us consider a single component of the sum in (10), and let

$$d_q(x_i, y_i) = A_q \cos(\Phi_q(x_i, y_i)) \quad (19)$$

denote this component. The question then is what are the conditions that ensure that A_q can indeed be interpreted as the instantaneous amplitude of $d_q(x_i, y_i)$ and $\Phi_q(x_i, y_i)$ as its phase.

Clearly, starting from a given signal $d_q(x_i, y_i)$, it is possible to introduce an infinite number of pairs $[a_q(x_i, y_i), \Phi_q(x_i, y_i)]$ such that $d_q(x_i, y_i) = a_q(x_i, y_i) \cos(\Phi_q(x_i, y_i))$. Nevertheless, in order to be able to interpret $a_q(x_i, y_i)$ as the instantaneous amplitude of the signal, and $\Phi_q(x_i, y_i)$ as its instantaneous phase, the instantaneous phase and amplitude should be defined in such a way that only a *single*, well defined, pair $[a_q(x_i, y_i), \Phi_q(x_i, y_i)]$ will correspond to the given signal $d_q(x_i, y_i)$. Similarly to the 1-D case, [22], the way to define without ambiguity the instantaneous amplitude and phase of a real signal $d_q(x_i, y_i)$ is to associate it with its *analytic signal*

$$z_q(x_i, y_i) = a_q(x_i, y_i) \exp(j\Phi_q(x_i, y_i)) \quad (20)$$

through the 2-D Hilbert transform [20], [21]. However, the 2-D Hilbert transform, [20], is uniquely defined only in cases where the signal energy is concentrated in the first and third quadrants of the spectral domain. More specifically, let $D_q(\omega, \nu)$ denote

the Fourier transform of $d_q(x_i, y_i)$. Then, it can be easily verified that a consistent definition of the 2-D Hilbert transform (that results in a nonnegative instantaneous amplitude) is possible only if

$$D_q(\omega, \nu) = 0, \quad \omega < 0, \quad \nu > 0 \quad \text{and} \quad \omega > 0, \quad \nu < 0. \quad (21)$$

Thus, in case the energy of $d_q(x_i, y_i)$ is concentrated in the second and fourth quadrants, the image must first be rotated by 90 degrees, so that its energy is concentrated in the first and third quadrants. We therefore conclude that it is required that $d_q(x_i, y_i)$ has its energy in two of the four quadrants only, either the first and third, or the second and fourth. Two-dimensional sinusoids have this property, and in most cases signals obtained by geometric distortions of sinusoids still possess this property.

Let $H[\cdot]$ denote the 2-D Hilbert transform operator. The analytic signal $z_q(x_i, y_i)$ of a real signal $d_q(x_i, y_i)$ whose energy is concentrated in the first and third quadrants of the frequency plane is obtained by applying the operator

$$M[\cdot] = (1 + jH[\cdot]) \quad (22)$$

to $d_q(x_i, y_i)$. Conversely, it is clear that $d_q(x_i, y_i) = \text{Re}\{z_q(x_i, y_i)\}$. In terms of spectral characterization, the analytic signal $z_q(x_i, y_i)$, is obtained from $d_q(x_i, y_i)$ by filtering it using a filter with frequency response equal to 2 for $\omega > 0, \nu > 0$ and zero elsewhere. Hence $z_q(x_i, y_i)$ is an analytic signal if its Fourier transform is nonzero only for $\omega > 0$ and $\nu > 0$. Thus $z_q(x_i, y_i)$ cannot be a real function, and therefore it has a unique amplitude-phase representation in the form (20), where the instantaneous amplitude is nonnegative. In conclusion, using the analytic signal we can associate with any real signal $d_q(x_i, y_i)$, satisfying the foregoing constraints, a unique pair of functions $[a_q(x_i, y_i), \Phi_q(x_i, y_i)]$, such that $a_q(x_i, y_i)$ is its instantaneous amplitude, and $\Phi_q(x_i, y_i)$ is its instantaneous phase.

The estimation algorithm summarized in Section III is designed to work with complex valued constant amplitude polynomial phase monocomponent signals. In our application the 2-D signal is real, and in general it has more than a single component. Thus the proposed algorithm for estimating the tilt and slant angles first isolates a single component from the observed signal and converts it into a complex form through the 2-D Hilbert transform. The problem then is how to best choose this component.

The component selection procedure is based on the results of [29] on the Cramer–Rao lower bound on the error variance in estimating the tilt and slant of the observed surface. Based on these results we conclude that the bounds are nearly linear functions of $1/\text{SNR}$, where SNR denotes the signal to noise ratio of the selected sinusoidal component of the surface texture. (See also Fig. 7.) It is further shown in [29] that the bounds on both the tilt and slant parameters are high when the center frequencies of the observed nonhomogeneous components are low. The bounds rapidly decrease as the spatial frequencies become higher. Hence, the selection rule selects the highest energy component among those components whose spatial frequency is away from DC. In other words, it may very well be, that a

higher frequency component will be chosen even if its amplitude is lower than that of a lower frequency component. Moreover, the filtering associated with the 2-D Hilbert transform can cause significant distortions if there is large energy in the low frequencies (near the DC). Hence, usage of a low frequency component should be avoided.

The selection result is verified using the CRLB by substituting the estimates obtained based on the alternative choices into the CRLB equations. The estimate that provides the lowest CRLB is chosen.

Once the definition of the analytic signal and the associated instantaneous amplitude and phase are given, we can return to the basic question posed at the beginning of this section, i.e., whether $\Phi_q(x_i, y_i)$ in (11) satisfies the conditions so that $\exp(j\Phi_q(x_i, y_i))$ is an analytic signal, or in other words whether the Fourier transform of $\exp(j\Phi_q(x_i, y_i))$ vanishes for $\omega < 0$ and for $\nu < 0$. This condition guarantees that the selected component indeed admits the representation of the form (19). In practice, the process of isolating a single component of (10), such that its frequency is away from DC implies that all low frequency components are filtered out in the conversion process. As a consequence, the Fourier transform of the resulting complex valued monocomponent signal is guaranteed to vanish for $\omega < 0$ and for $\nu < 0$.

V. TILT AND SLANT ESTIMATION BASED ON A TAYLOR SERIES EXPANSION OF THE PHASE

In Section II it is shown that the perspective transformation transforms the homogeneous surface texture into a nonhomogeneous texture in the image plane. Thus under the perspective transformation the phase of a harmonic component whose phase function is given, in surface coordinates, by $\Phi_s(x_s, y_s) = \omega x_s + \nu y_s + \varphi$ becomes after expressing x_s and y_s in terms of x_i and y_i using (8)

$$\begin{aligned} \Phi(x_i, y_i) &= \frac{x_i(\tilde{u} \cos \tau - \tilde{v} \cos \sigma \sin \tau) + y_i(\tilde{u} \sin \tau + \tilde{v} \cos \sigma \cos \tau) + \varphi}{\sin \sigma(x_i \cos \tau + y_i \sin \tau) + f \cos \sigma} \end{aligned} \quad (23)$$

in the coordinate system of the observed image.

In this section we present a computationally efficient algorithm for estimating the slant and the tilt of the planar surface directly from the estimated polynomial model of the phase function $\Phi(x_i, y_i)$. In order to do so we assume that the estimated polynomial of total degree K is in fact, the K th order Taylor series expansion of the phase.

Let us assume for a moment that x_i and y_i are continuous variables. Since the phase function (23) is infinitely differentiable it can be expanded into a Taylor series about (x_0, y_0) . Hence

$$\begin{aligned} \Phi(x_i, y_i) &= \Phi(x_0, y_0) + \sum_{n=1}^K \frac{1}{n!} d^n \Phi(x_0, y_0) \\ &+ \frac{1}{(K+1)!} d^{K+1} \Phi(x_1, y_1) \end{aligned} \quad (24)$$

where (x_1, y_1) is a point on the line that connects (x_0, y_0) with (x_i, y_i) . The n th order differential $d^n \Phi(x, y)$ about (x_0, y_0) is defined by

$$d^n \Phi(x_0, y_0) = \left[(x_i - x_0) \frac{\partial}{\partial x_i} + (y_i - y_0) \frac{\partial}{\partial y_i} \right]^n \Phi(x_0, y_0). \quad (25)$$

Let $N(x_i, y_i)$ denote the numerator of the phase function expression in (23), and let

$$D(x_i, y_i) = \frac{1}{\sin \sigma(x_i \cos \tau + y_i \sin \tau) + f \cos \sigma}. \quad (26)$$

We therefore have that

$$\frac{\partial^{(k+l)} D(x_0, y_0)}{\partial x_i^k \partial y_i^l} = (-1)^{(k+l)} (k+l)! t_1^k t_2^l D(x_0, y_0) \quad (27)$$

where we define

$$t_1 = \frac{\cos \tau \sin \sigma}{\sin \sigma(x_0 \cos \tau + y_0 \sin \tau) + f \cos \sigma} \quad (28)$$

and

$$t_2 = \frac{\sin \tau \sin \sigma}{\sin \sigma(x_0 \cos \tau + y_0 \sin \tau) + f \cos \sigma}. \quad (29)$$

Lemma 1: The general term of the Taylor series expansion of $D(x_i, y_i)$ is given by

$$\begin{aligned} \frac{1}{n!} d^n D(x_0, y_0) &= (-1)^n D(x_0, y_0) (t_1(x_i - x_0) + t_2(y_i - y_0))^n. \end{aligned} \quad (30)$$

Proof: Using equation (27) we have that

$$\begin{aligned} \frac{1}{n!} d^n D(x_0, y_0) &= \frac{1}{n!} \sum_{l=0}^n \binom{n}{l} \frac{\partial^n D(x_0, y_0)}{\partial x_i^{n-l} \partial y_i^l} (x_i - x_0)^{n-l} (y_i - y_0)^l \\ &= \frac{(-1)^n}{n!} D(x_0, y_0) \sum_{l=0}^n n! \binom{n}{l} t_1^{n-l} t_2^l \\ &\quad \cdot (x_i - x_0)^{n-l} (y_i - y_0)^l \\ &= (-1)^n D(x_0, y_0) (t_1(x_i - x_0) + t_2(y_i - y_0))^n. \end{aligned} \quad (31)$$

Expanding (26) into a Taylor series about (x_0, y_0) , while keeping terms up to the K th order, we obtain

$$\begin{aligned} D_K(x_i, y_i) &= D(x_0, y_0) \left[1 + \sum_{n=1}^K (-1)^n (t_1(x_i - x_0) + t_2(y_i - y_0))^n \right]. \end{aligned} \quad (32)$$

Since the numerator is a polynomial of total-degree 1, its Taylor series expansion is given by

$$N(x_i, y_i) = c + (x_i - x_0)c_1 + (y_i - y_0)c_2 \quad (33)$$

where we define

$$c_1 = \tilde{u} \cos \tau - \tilde{v} \cos \sigma \sin \tau, \quad (34)$$

$$c_2 = \tilde{u} \sin \tau + \tilde{v} \cos \sigma \cos \tau \quad (35)$$

and

$$c = c_1 x_0 + c_2 y_0. \quad (36)$$

Let $\Phi_K(x_i, y_i)$ denote the K th order Taylor series expansion of the phase function (23). Since the expansion of $\Phi(x_i, y_i)$ into a Taylor series form about (x_0, y_0) is unique, an expression for $\Phi_K(x_i, y_i)$ can now be found by multiplying the Taylor series expansion of the phase numerator, $N(x_i, y_i)$, by $D_K(x_i, y_i)$, and adding to it the constant phase term φ . (Note that the multiplication produces an additional term of order $K + 1$ which is omitted.) Using (31) and (33) we conclude that $\Phi_K(x_i, y_i)$ has the general form

$$\Phi_K(x_i, y_i) = \sum_{(n,m) \in I} c(n, m)(x_i - x_0)^n (y_i - y_0)^m \quad (37)$$

where

$$I = \{0 \leq n, m \text{ and } n + m \leq K\}. \quad (38)$$

The coefficients $c(n, m)$ are a result of collecting all the components that include $(x_i - x_0)^n (y_i - y_0)^m$ after the multiplication of $N(x_i, y_i)$ and $D_K(x_i, y_i)$. More specifically, as shown in (39) at the bottom of the page.

Our goal in this section is to find the slant and the tilt of the observed planar surface using only the estimated expansion coefficients $c(n, m)$. Substituting the estimated coefficients $c(n, m)$, $(n, m) \in I$, into (39) we obtain a system of equations which is highly nonlinear in the tilt and slant parameters. Note however that in order to find the tilt and slant angles it is sufficient to evaluate t_1 and t_2 , as t_1 and t_2 are functions of the unknown tilt and slant angles, and other known quantities. (Observe that c_1 and c_2 are functions of the unknown tilt and slant, as well as of the unknown frequency parameters \tilde{u}, \tilde{v} . These parameters, however, are not part of the problem of finding the orientation of a planar surface.)

The next theorem establishes a *linear and recursive* relation between the coefficients of the Taylor series expansion of the phase and the unknown quantities t_1 and t_2 . This linear relation enables us to derive a computationally efficient algorithm for estimating the tilt and the slant from the expansion coefficients.

Theorem 2: Let K be some positive integer, and let $c(n, m)$, $(n, m) \in I$ be the coefficients of the K th order Taylor series

expansion of the phase function, $\Phi(x_i, y_i)$. Then,

$$c(n, m) = -c(n-1, m)t_1 - c(n, m-1)t_2, \quad (40)$$

$$n + m \geq 2 \text{ and } n, m \geq 0$$

where $c(n, m) = 0$ when $n < 0$ or $m < 0$.

Proof: By induction. We first consider the case where $n \geq 2$ and $m = 0$. Evaluating the right hand-side of (40) using (39) we have

$$-c(n-1, 0)t_1 = D(x_0, y_0)(-1)^n [ct_1^n - c_1 t_1^{n-1}] = c(n, 0). \quad (41)$$

For the case where $m \geq 2$ and $n = 0$, a similar substitution yields

$$-c(0, m-1)t_2 = D(x_0, y_0)(-1)^m [ct_2^m - c_2 t_2^{m-1}] = c(0, m). \quad (42)$$

For the general case, i.e., $n \geq 1$ and $m \geq 1$, we have

$$\begin{aligned} & -c(n-1, m)t_1 - c(n, m-1)t_2 \\ &= D(x_0, y_0)(-1)^{n+m} c \\ & \cdot \left[\binom{n+m-1}{n} + \binom{n+m-1}{n-1} \right] t_1^n t_2^m \\ & - D(x_0, y_0)(-1)^{n+m} c_1 \\ & \cdot \left[\binom{n+m-2}{n-2} + \binom{n+m-2}{n-1} \right] t_1^{n-1} t_2^m \\ & - D(x_0, y_0)(-1)^{n+m} c_2 \\ & \cdot \left[\binom{n+m-2}{n-1} + \binom{n+m-2}{n} \right] t_1^n t_2^{m-1} \\ &= c(n, m) \end{aligned} \quad (43)$$

where the last equality is due to the identity

$$\binom{l}{k} + \binom{l}{k+1} = \binom{l+1}{k+1}. \quad (44)$$

Since in practice the coefficients of the Taylor series expansion are unknown, they have to be replaced by their estimates. In order to do so we assume that the estimated polynomial of total degree K is in fact, the K th order Taylor series expansion of the phase. Hence, in this case (40) holds only approximately. Thus, rewriting (40) we have

$$c(n, m) = -c(n-1, m)t_1 - c(n, m-1)t_2 - c(n, m), \quad (45)$$

$$n + m \geq 2 \text{ and } n, m \geq 0$$

$$c(n, m) = D(x_0, y_0) \begin{cases} (-1)^n [ct_1^n - c_1 t_1^{n-1}], & n \geq 1, m = 0 \\ (-1)^m [ct_2^m - c_2 t_2^{m-1}], & m \geq 1, n = 0 \\ (-1)^{n+m} \left[c \binom{n+m}{n} t_1^n t_2^m - c_1 \binom{n+m-1}{n-1} t_1^{n-1} t_2^m - c_2 \binom{n+m-1}{n} t_1^n t_2^{m-1} \right], & n \geq 1, m \geq 1 \end{cases} \quad (39)$$

where $c(n, m) = 0$ when $n < 0$ or $m < 0$. Here, $c(n, m)$ denotes the approximation error.

Let $\mathbf{T} = [t_1 \ t_2]^T$. Also, let

$$\mathbf{C} = - \begin{bmatrix} c(1, 0) & 0 \\ c(0, 1) & c(1, 0) \\ 0 & c(0, 1) \\ c(2, 0) & 0 \\ \vdots & \vdots \\ 0 & c(0, k-1) \end{bmatrix} \quad \mathbf{b} = \begin{bmatrix} c(2, 0) \\ c(1, 1) \\ c(0, 2) \\ c(3, 0) \\ \vdots \\ c(0, k) \end{bmatrix}. \quad (46)$$

We thus obtain the following *linear* system of equations

$$\mathbf{C}\mathbf{T} - \mathbf{b} = \mathbf{e} \quad (47)$$

where \mathbf{e} is the approximation error vector. The desired parameters t_1 and t_2 can now be found by minimizing the sum of the squared approximation error. The solution to this linear least squares problem is given by

$$\mathbf{T} = [\mathbf{C}^T \mathbf{W} \mathbf{C}]^{-1} \mathbf{C}^T \mathbf{W} \mathbf{b} \quad (48)$$

where \mathbf{W} is an optional weighting matrix.

Having estimated \mathbf{T} there are four possible pairs of slant and tilt angles that satisfy (28) and (29)

$$\sigma, \tau = \begin{cases} \tau_1, \sigma_1 \\ \tau_1, \sigma_1 + \pi \\ \tau_1 + \pi, -\sigma_1 \\ \tau_1 + \pi, -\sigma_1 + \pi \end{cases} \quad (49)$$

where σ_1 and τ_1 are given by

$$\tau_1 = \arctan\left(\frac{t_2}{t_1}\right) \quad (50)$$

and

$$\sigma_1 = \operatorname{arccot}\left[\frac{1}{f}\left(\frac{\sin \tau_1}{t_2} - x_0 \cos \tau_1 - y_0 \sin \tau_1\right)\right]. \quad (51)$$

However, only a *single* solution out of the four possible ones satisfies the condition $0 \leq \sigma < \pi/2$. This solution is the required one.

We have thus established a computationally efficient algorithm for estimating the tilt and the slant angles of the observed planar surface. Having estimated the 2-D polynomial model of the observed signal phase using the PD algorithm, the original, highly nonlinear, slant and tilt estimation problem is reduced to the linear least-squares problem (48). The computational attractiveness of the proposed algorithm is due to the fact that estimation of the phase model parameters is accomplished using FFTs. The estimation of the tilt and slant in the second stage requires only the solution of a linear system of equations, whose coefficients are the estimated coefficients of the polynomial phase. In particular, there is no need for an iterative solution. However, as we show in Section VII, the algorithm though computationally efficient, has a relatively high error variance.

VI. IMPROVING THE ACCURACY OF THE TAYLOR SERIES BASED ALGORITHM

The inaccuracy of the estimation algorithm that employs the Taylor series expansion of the phase function, is due to the implicit assumption that the 2-D polynomial phase estimated using the PD algorithm is, in fact, the K th order Taylor series expansion of the phase. Improved estimation algorithms are required in cases where the performance of the Taylor series expansion based algorithm is not acceptable. This algorithm can then serve to initialize a computationally more complex algorithm.

In the case of continuous index fields, the local spatial frequencies are the partial derivatives of the local phase function. In [14] the relation between the local spatial frequency in the image coordinate system, $\mathbf{u}_i = [u_i, v_i]^T$, and the local spatial frequency in the surface coordinate system, $\mathbf{u}_s = [\omega, \nu]^T$, is derived. This relation is given by

$$\begin{aligned} \mathbf{u}_i &= \nabla \Phi(\mathbf{x}_i) = \nabla \left[[\mathbf{x}_s(\mathbf{x}_i)]^T \mathbf{u}_s \right] \\ &= \begin{bmatrix} \frac{\partial x_s}{\partial x_i} & \frac{\partial y_s}{\partial x_i} \\ \frac{\partial x_s}{\partial y_i} & \frac{\partial y_s}{\partial y_i} \end{bmatrix} \mathbf{u}_s \end{aligned} \quad (52)$$

where the operator ∇ is defined by

$$\nabla = \begin{bmatrix} \frac{\partial}{\partial x_i} & \frac{\partial}{\partial y_i} \end{bmatrix}^T. \quad (53)$$

Inverting (52) we have

$$\mathbf{u}_s = \mathbf{H} \mathbf{u}_i \quad (54)$$

where

$$\begin{aligned} \mathbf{H} &= \frac{\sin \sigma}{z_0 - x_s \sin \sigma} \begin{bmatrix} x_i & y_i \\ 0 & 0 \end{bmatrix} \\ &+ \frac{f}{z_0 - x_s \sin \sigma} \begin{bmatrix} \cos \sigma \cos \tau & \cos \sigma \sin \tau \\ -\sin \tau & \cos \tau \end{bmatrix}. \end{aligned} \quad (55)$$

Thus, assuming for a moment x_i and y_i to be continuous variables the estimated local spatial frequencies of the signal are the partial derivatives of its estimated local phase function $\Phi(\mathbf{x}_i)$ of total-degree K , i.e.,

$$\begin{aligned} u_i(x_i, y_i) &= \frac{1}{2\pi} \frac{\partial \Phi(x_i, y_i)}{\partial x_i} \\ &= \frac{1}{2\pi} \sum_{(k, \ell) \in \{1 \leq k; 0 \leq \ell; 1 \leq k + \ell \leq K\}} c(k, \ell) k x_i^{k-1} y_i^\ell, \end{aligned} \quad (56)$$

and

$$\begin{aligned} v_i(x_i, y_i) &= \frac{1}{2\pi} \frac{\partial \Phi(x_i, y_i)}{\partial y_i} \\ &= \frac{1}{2\pi} \sum_{(k, \ell) \in \{0 \leq k; 1 \leq \ell; 1 \leq k + \ell \leq K\}} c(k, \ell) \ell x_i^k y_i^{\ell-1}. \end{aligned} \quad (57)$$

Having estimated the polynomial phase model coefficients, $\{c(k, \ell)\}$, we obtain by substituting the estimated parameters

into (56) and (57) an estimate of the spatial frequencies of the selected harmonic component.

By assumption, in the surface coordinate system, the spatial frequencies ω and ν of the selected harmonic component are constants. Thus the improvement algorithm searches for the σ and τ values that result in a minimal variation of \mathbf{u}_s . More specifically, for any hypothesized value of the surface orientation σ, τ , we back-project the estimated spatial frequency \mathbf{u}_i of the selected image component onto the hypothesized planar surface using (54) and compute the variance of \mathbf{u}_s on the entire planar surface. The values of σ and τ that minimize the variance provide the estimate of the surface orientation. The cost function which is to be minimized is given by

$$V_{\sigma, \tau} = \sum_{x_i, y_i} \left[\hat{\omega}(x_i, y_i) - \frac{1}{N} \sum_{x_i, y_i} \hat{\omega}(x_i, y_i) \right]^2 + \sum_{x_i, y_i} \left[\hat{\nu}(x_i, y_i) - \frac{1}{N} \sum_{x_i, y_i} \hat{\nu}(x_i, y_i) \right]^2 \quad (58)$$

where $\hat{\omega}(x_i, y_i)$ and $\hat{\nu}(x_i, y_i)$ are the results of back-projecting the estimated spatial frequencies $u_i(x_i, y_i)$ and $v_i(x_i, y_i)$ of (56) and (57), evaluated at some image coordinate (x_i, y_i) , onto the hypothesized planar surface using (54). Here, N denotes the number of samples of the observed image, used to evaluate the mean. (Clearly, the mean can be evaluated using the entire image of the observed surface.)

To reduce the computational load required by such an exhaustive multidimensional grid search we apply the Taylor series based estimation procedure to obtain an initial approximated estimate of the problem parameters. The minimization procedure is then applied only in a small neighborhood of the estimated parameters to refine these estimates.

VII. NUMERICAL EXAMPLES

In this section we illustrate the performance of the proposed parametric methods for estimating the tilt and slant of a textured planar surface by applying the algorithms to synthetic as well as to photographed images. Monte-Carlo simulations are performed to analyze the statistical properties of the algorithms.

A. Application of the Algorithms of Synthetic Data

Fig. 2 shows an image of a planar surface slanted into the page such that $\sigma = 60^\circ$ and $\tau = 90^\circ$. The observation noise is a zero mean, additive white Gaussian noise. The surface texture has six harmonic components and is given by

$$t(x_s, y_s) = \sin(x_s\omega_0 + y_s\nu_0) + \frac{1}{3} \sin(3x_s\omega_0 + 3y_s\nu_0) + \frac{1}{5} \sin(5x_s\omega_0 + 5y_s\nu_0) + \sin(-x_s\omega_0 + y_s\nu_0) + \frac{1}{3} \sin(-3x_s\omega_0 + 3y_s\nu_0) + \frac{1}{5} \sin(-5x_s\omega_0 + 5y_s\nu_0) \quad (59)$$

where $(\omega_0, \nu_0) = (0.15, 0.15)$ cycles/cm. To generate the image of the planar surface, the intensity of each pixel in the image plane was evaluated by projecting the intensity levels of the surface texture using (8). More specifically, the intensity of each image pixel (x_i, y_i) is that of the surface coordinate

which is mapped by the perspective projection to (x_i, y_i) . The focal length of the camera is $f = -60$ mm, $z_0 = 6$ m, and the image plane dimensions are 30 mm \times 30 mm, with the origin being located at the center of the image plane.

Define

$$\text{SNR}_D = \frac{A_D^2}{\sigma^2} \quad (60)$$

where A_D is the amplitude of the selected harmonic component (the dominant one in this example) and σ^2 is the variance of the observation noise. In this example we demonstrate the operation of the proposed algorithms on a 64×64 image taken from the center of the image in Fig. 2, where $\text{SNR}_D = 20$ dB.

Fig. 3 depicts the discrete Fourier transform (DFT) of the 64×64 image taken from the center of the image in Fig. 2. It is clear that the harmonic structure of the Fourier transform of the homogeneous surface texture does not exist anymore in the Fourier transform of the observed nonhomogeneous image.

In the initial step of the proposed algorithms the selected harmonic component is separated from the other components of the signal, and transformed into an analytic signal. To isolate the selected component of the signal and to convert it into the complex form $\exp(j\Phi(x_i, y_i))$ the image is filtered by the filter whose design procedure is described in Section IV. In the absence of noise, the root mean squared error between the complex valued selected component of the signal calculated analytically and the signal produced by the filtering procedure is 0.15% of the signal magnitude.

To illustrate the operation of the phase estimation algorithm, Fig. 4 depicts the observed and estimated phase of the selected component of the nonhomogeneous signal. Note the continuity of the estimated phase despite the 2π discontinuities of the observed phase. The estimated polynomial, $\hat{P}(x_i, y_i)$, is of total-degree 3. The left hand-side of Fig. 5 shows a noise free image of the selected component. The right hand-side image shows the signal $\sin(\hat{P}(x_i, y_i))$ estimated using the PD algorithm, in the presence of noise. The results indicate that the synthesized image is indistinguishable from the original. Having estimated the phase, we can apply the proposed algorithms to estimate the tilt and the slant of the observed surface.

1) *Algorithm 1—Tilt and Slant Estimation Based on a Taylor Series Expansion:* Using this algorithm, the orientation of the planar surface is estimated directly from the estimated polynomial phase coefficients $\hat{c}(n, m)$, obtained by the PD algorithm. In Table I, we compare the estimated coefficients with the Taylor series expansion coefficients evaluated using (39). The expansion coefficients are evaluated around the origin of the image coordinate system since this is the $(0, 0)$ coordinate used by the PD algorithm, as well.

Comparing the estimated coefficients with the coefficients of the Taylor series expansion it can be seen that the assumption that the estimated polynomial $\hat{P}(x_i, y_i)$ approximates a third order Taylor series expansion of the phase, holds better for coefficients in lower layers of the phase model while larger errors are found in higher layers. Substituting the estimated coefficients to (48)–(51) we obtain $\sigma = 58.66^\circ$ and $\tau = 89.56^\circ$.

2) *Algorithm 2—Improving the Accuracy of Algorithm 1 Through the Minimization of a Cost Function:* This algorithm

searches for the σ and τ pair that minimizes an estimate of the variance of the local spatial frequency of the surface texture using (58). To reduce the computational load required by such an exhaustive multidimensional grid search we use the results of the first algorithm as an initial estimate. Thus, the search is performed only in a region of $\pm 10^\circ$ around the estimated σ, τ produced by the first algorithm. Fig. 6 depicts the cost function $V_{\sigma, \tau}$ in the region searched by the algorithm.

The algorithm performs the grid search in few iterations, where in each iteration the resolution is divided by 4. In the specific example shown here, the estimated values are $\sigma = 60.33^\circ$ and $\tau = 89.85^\circ$.

B. Statistical Performance Analysis of the Estimation Algorithms

In this subsection we illustrate the performance of the proposed parameter estimation algorithms using Monte Carlo simulations. We compare the variance of the estimation errors of the suggested algorithms with the CRLB derived in [29]. The surface texture being considered in this example has three sinusoidal components and is given by

$$t(x_s, y_s) = \sin(x_s \omega_0 + y_s \nu_0) + \frac{1}{3} \sin(3x_s \omega_0 + 3y_s \nu_0) + \frac{1}{5} \sin(5x_s \omega_0 + 5y_s \nu_0) \quad (61)$$

where $(\omega_0, \nu_0) = (0.25, 0)$ cycles/cm. The surface orientation parameters are $\sigma = 30^\circ$ and $\tau = 90^\circ$. The observation noise is a zero mean, additive white Gaussian noise. We investigate the performance of the algorithms as a function of the selected component signal to noise ratio SNR_D , and as a function of the dimensions of the observed image.

The experimental standard deviation results depicted in Fig. 7 are based on 500 independent realizations of the image for each SNR_D and data dimensions. Since the CRLB is a lower bound on the error variance of any unbiased estimator of the problem parameters, the Monte Carlo results in Fig. 7 are depicted only for cases where the experimental bias is much smaller than the standard deviation. For smaller values of SNR_D and data dimensions, both algorithms become biased. The results indicate that the refined estimates obtained by applying the iterative minimization procedure are considerably less biased and are of lower error variance than the initial estimates obtained using the algorithm based on the Taylor series expansion.

From Fig. 7 we conclude that even for low SNRs and moderate dimensions of the observed image (40×40 pixels), the error variance of Algorithm 2 is about 6–7 dB away from the CRLB. The Taylor series expansion based algorithm (Algorithm 1), is considerably less accurate and its error variance is around 20 dB away from the CRLB. We therefore recommend to use it only to initialize Algorithm 2.

C. Experimental Results with Photographed Textured Surfaces

In this subsection we evaluate the performance of the algorithms by applying them to photographed textured surfaces. The images are those used in [14]. The prior knowledge required in order to apply the algorithms is the focal length of the camera and the image coordinate system in common units. The

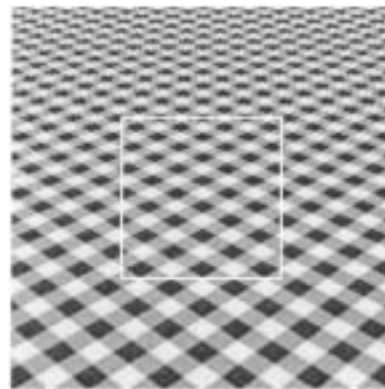


Fig. 2. Noisy image of a planar surface slanted into the page with $\sigma = 60^\circ$. The algorithms are applied only to the pixels in the center square.

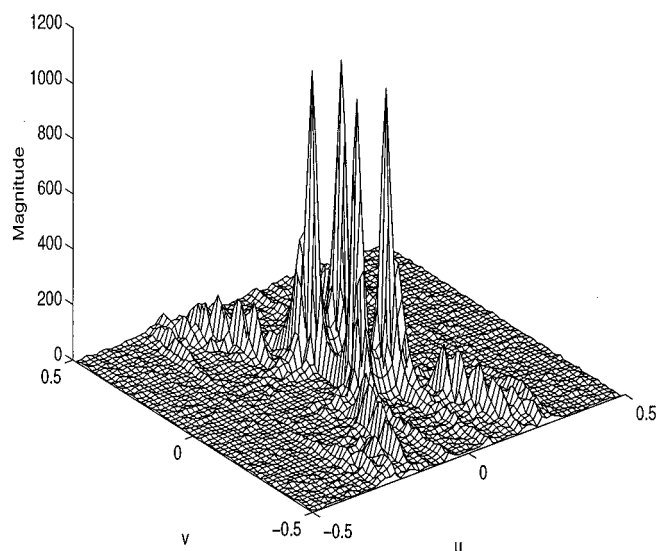


Fig. 3. Fourier transform of the image.

algorithms were applied to a 64×64 segment of each original 128×128 image. Fig. 8 shows the images, the estimated orientation produced by each of the proposed algorithms, the measured (“true”) orientation and an ellipse that illustrates the estimation results of Algorithm 2. Note that the measured tilt τ_T and slant σ_T are subject to a measurement error of 1° – 3° .

The experimental results suggest that both algorithms are useful for estimating the orientation parameters of planar textured surfaces, for textures containing structural components. Note however that as $\sigma \rightarrow 0$ the tilt is losing its physical meaning. Moreover, analysis of the CRLB on estimating the tilt and slant angles, [29], indicates that the lower bound on estimating the tilt angle becomes very high as the slant tends to zero. We therefore emphasize that estimated tilt values should be considered meaningless when the corresponding estimated slant values tend to zero. (Thus, in Fig. 8 such cases are indicated by $\tau_T = -$.) As previously concluded from the statistical performance analysis of the algorithms, the accuracy of the algorithm based on the Taylor series expansion is lower, but it is computationally much more attractive than the iterative procedure.

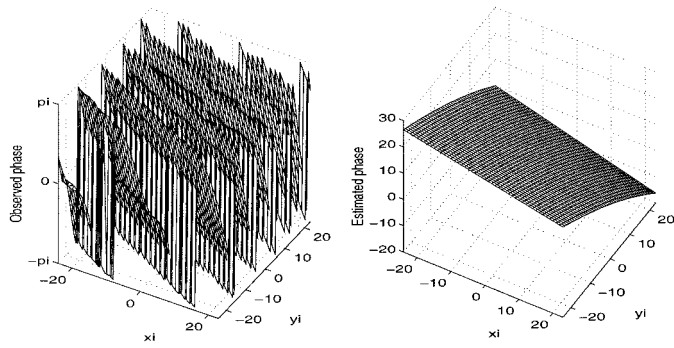


Fig. 4. Observed and estimated phase functions of the selected component of the image plane nonhomogeneous texture.

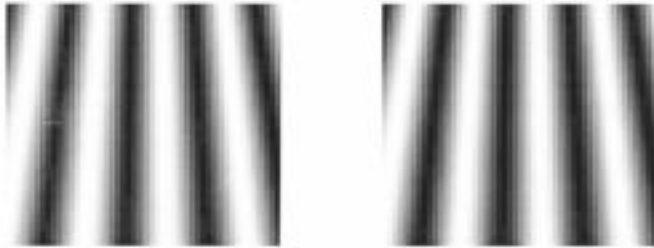


Fig. 5. (Left) Image of a planar surface where the surface texture comprises only the selected harmonic component. (Right) Synthesized surface image obtained from the phase estimated using the PD algorithm.

TABLE I
COMPARISON BETWEEN THE POLYNOMIAL PHASE COEFFICIENTS AND THE TAYLOR SERIES EXPANSION COEFFICIENTS

Layer	Coefficient	The estimated coefficients	Theoretical Taylor coefficients
0	$c(0,0)$	$-4.99462 \cdot 10^{-1}$	$-5.04156 \cdot 10^{-1}$
1	$c(1,0)$	$-3.46070 \cdot 10^{-1}$	$-3.48256 \cdot 10^{-1}$
1	$c(0,1)$	$7.49375 \cdot 10^{-1}$	$7.52529 \cdot 10^{-1}$
2	$c(2,0)$	$-4.92818 \cdot 10^{-5}$	0
2	$c(1,1)$	$2.21451 \cdot 10^{-3}$	$2.33407 \cdot 10^{-3}$
2	$c(0,2)$	$-4.75581 \cdot 10^{-3}$	$-5.04359 \cdot 10^{-3}$
3	$c(3,0)$	$3.03372 \cdot 10^{-7}$	0
3	$c(2,1)$	$9.55789 \cdot 10^{-7}$	0
3	$c(1,2)$	$-1.03960 \cdot 10^{-5}$	$-1.56434 \cdot 10^{-5}$
3	$c(0,3)$	$2.09085 \cdot 10^{-5}$	$-2.26554 \cdot 10^{-7}$

D. Orthogonalization of a Perspective Viewed Image

Once the tilt and slant angles of the observed surface have been estimated it becomes possible to recover the homogeneous surface texture from the perspective viewed image of that surface, through nonuniform re-sampling of the observed image. Applying this procedure to the entire image, which the textured surface is part of, considerably simplifies further processing such as content-based indexing and retrieval of images. In the following we summarize the main steps of an algorithm for “orthogonalizing” the observed image so that the effect of the perspective projection is eliminated, and provide examples demonstrating the applicability of the proposed procedure to complex real-world colored images where the textured patch employed by the algorithm is only a small part of the entire image. The main steps of the orthogonalization procedure are as follows.

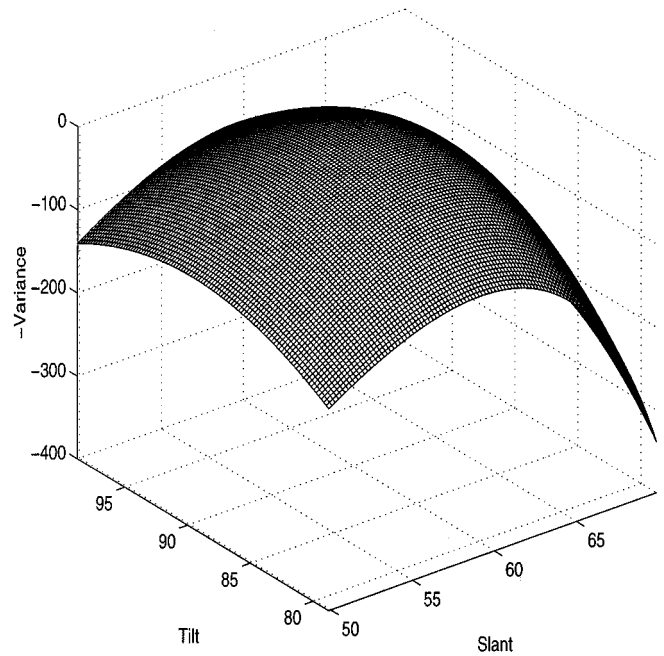


Fig. 6. Cost function $V_{\sigma, \tau}$ shown with an inverted sign.

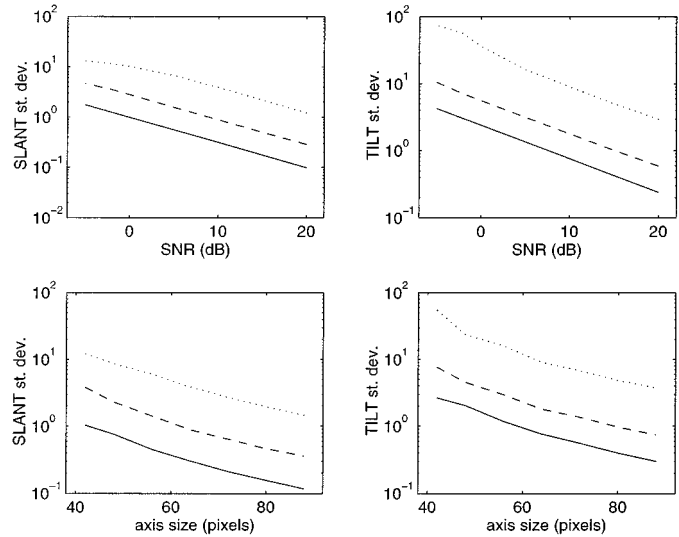


Fig. 7. Performance of the proposed algorithms as a function of SNR_D and data dimensions in comparison with the corresponding CRLB. Solid line denotes the CRLB, dotted line denotes the performance of the Taylor series expansion based algorithm (Algorithm 1), while dashed line denotes the performance after the iterative refinement stage (Algorithm 2).

- Estimate the orientation of the planar surface.
- Using the inverse coordinate transformation, (8), find the coordinates of the image boundaries, expressed in surface coordinates (at the desired scaling).
- Uniformly sample the surface coordinate system.
- Using (7) evaluate the image coordinate \mathbf{x}_i that corresponds to each \mathbf{x}_s on the surface sampling grid.
- For each of the RGB planes, the gray level of each sample in the surface coordinate system is set to the gray level of the corresponding observed image sample \mathbf{x}_i (using interpolation since in general the resulting x_i and y_i are not integers).

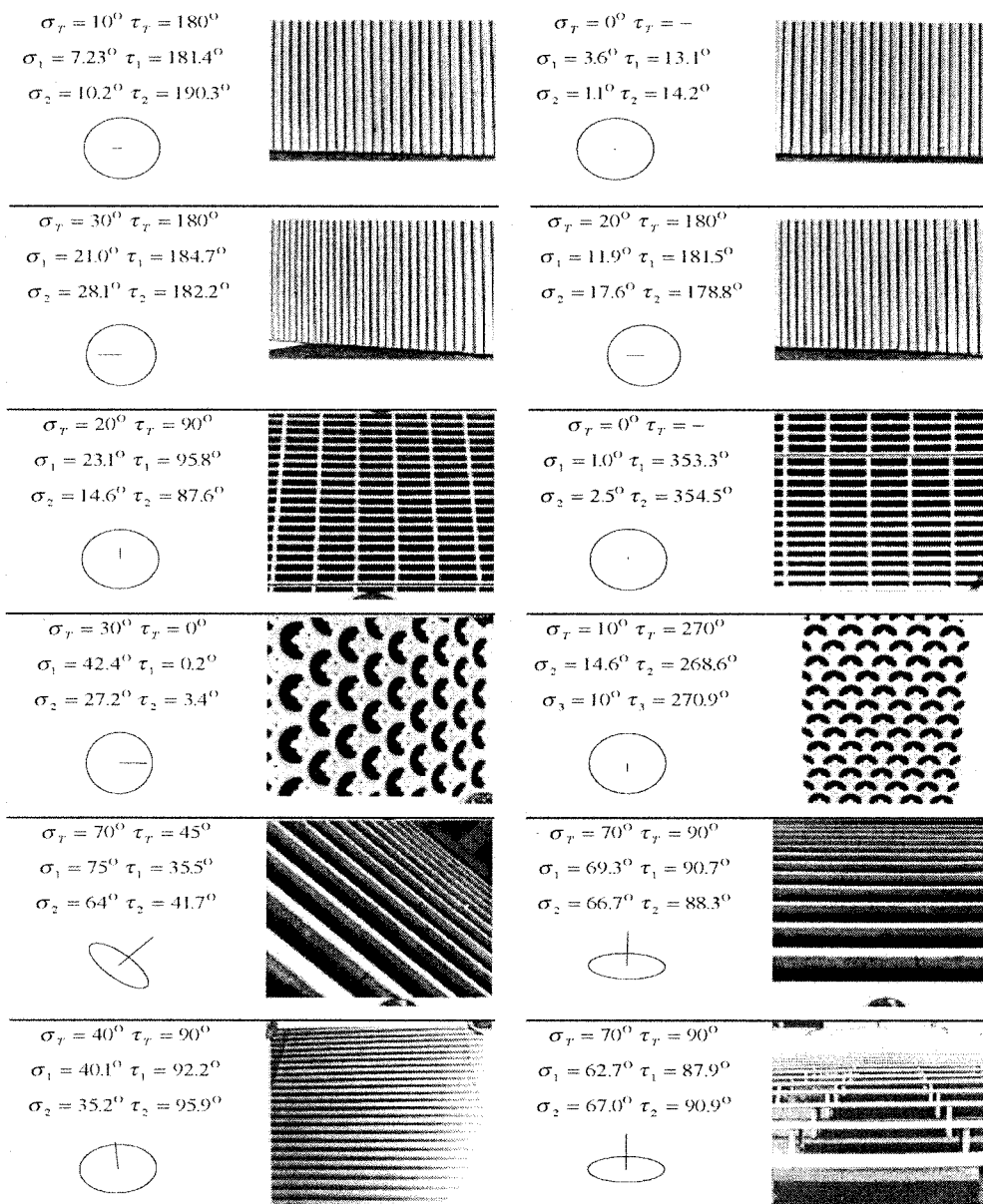


Fig. 8. The images and the corresponding estimated tilt and slant parameters. Here, τ_1 and σ_1 denote the estimated tilt and slant produced by the Taylor series expansion based algorithm, while τ_2 and σ_2 denote the estimated tilt and slant produced after the iterative refinement stage. The measured tilt τ_T and slant σ_T are given in the first row. Based on the estimated tilt and slant we depict the orientation of the surface normal as seen in the image plane. The ellipse illustrates how a circle drawn on the planar surface would appear in the image plane, based on the estimated tilt and slant.

Note that for the purpose of orthogonalizing the perspective projected image, knowledge of the focal length is not required. Hence, an arbitrary focal length can be assumed if the focal length is unknown. This is easily deduced using (8) as the focal length has only a uniform scaling effect on the mapping between the image coordinates \mathbf{x}_i and the surface coordinates \mathbf{x}_s that we would like to recover. Hence, assuming an arbitrary focal length f results in recovering the same surface \mathbf{x}_s , however in a different scale. Because the decision on the dimensions of the orthogonalized image is anyway an arbitrary user's choice, this scaling has no effect. On the other hand, knowledge of the optical center of the image is required by the orthogonalization procedure.

The results of applying this procedure to three real-world images taken from the VisTex library are shown in Fig. 9. Note

that since the building image in the middle column of Fig. 9 is composed of two planar surfaces, the image was manually segmented and the orthogonalization procedure was independently applied to each one of them in order to obtain the image in the middle of the bottom row. It is easily seen that the recovered textures are indeed nearly homogeneous.

Fig. 10, left column, depicts two aerial images taken from an unknown angle. Both images contain homogeneous textured regions that appear nonhomogeneous due to the perspective projection. Parts of these regions, marked using white squares, are employed to estimate the orientation of the surfaces. In the case of the stadium image the texture is that of cars parked in a parking lot, while in the case of the pier image the texture is composed of an array of rectangular structures. Since in these

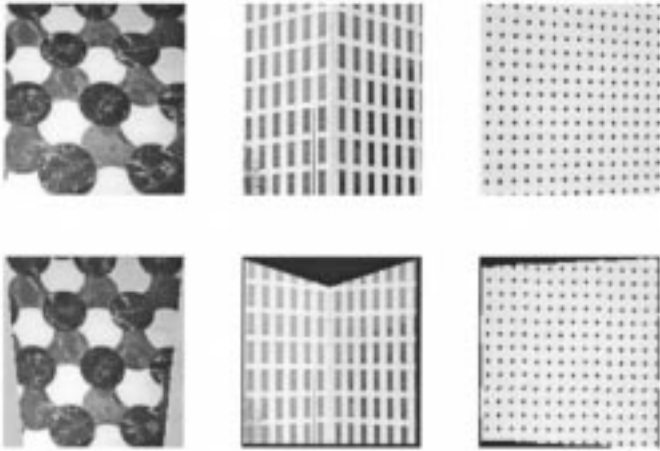


Fig. 9. Recovered homogeneous surface textures (bottom row) from the observed perspective projected images (top row).

images the optical center is unknown, we have arbitrarily assumed it to be in the middle of the image. To realize that the proposed procedure indeed produce the desired results, note for example that in the stadium image the cars get smaller at the top of the real image but are in a uniform size in the orthogonalized image. Also, in the orthogonalized image the stadium upper contour is symmetric and oval; the white field lines are either orthogonal or parallel to each other, contrary to their appearance in the perspective projected original. Note however that since our modeling assumption is that the observed surface is flat and planar, objects of nonnegligible height relative to their distance from the camera, cannot be perfectly orthogonalized by the proposed procedure. For example consider the surface generated by the spectators seats. This surface is not in the plane of the parking lot, nor in a parallel plane. Hence, in the orthogonalized image the surface of the spectators seats is not symmetrical as one would expect from a truly orthogonal image. The pier images illustrates some additional features of the proposed orthogonalization algorithm. Note in particular that the rounded structures on the top right of the pier image are seen in the real image as small oval structures while in the recovered image they appear as circles. Also, the oval shaped tracks on the top left part of the image, that can be hardly seen in the perspective viewed image, are clearly observed in the orthogonalized image. Moreover, as an illustration of the accuracy of the tilt and slant estimation procedure as well as that of the orthogonalization procedure, observe that the field of rectangular structures that is used for estimating the orientation of the surface indeed became a field of rectangular structures, as opposed to its distorted, perspective projected appearance in the observed image. Finally note that, as expected, in the orthogonalized image the distance of the pier from the parallel pier where the rectangular structures are located, is equal at any point along the pier.

VIII. CONCLUSIONS

We have presented a parametric solution to the problem of estimating the orientation in space of a planar textured surface, from a single, noisy, observed image of it. The proposed solution is based on the observation that the coordinate transformation

from surface to image coordinates, due to the perspective projection, uniquely transforms each homogeneous sinusoidal component of the surface texture into a sinusoid whose frequency is a function of location in the image coordinate system. Since the sinusoid phase is a continuous function of the field coordinates it can be approximated by a 2-D polynomial function of the field coordinates. Using the 2-D Hilbert transform and the PD algorithm we fit a constant-amplitude, polynomial-phase model to a sinusoidal component of the observed texture, such that the concepts of 2-D instantaneous phase, frequency, and amplitude are well defined. We then establish a linear recursive relation between the model parameters and the unknown slant and tilt. A linear least squares solution of the resulting system provides the slant and tilt estimates. To improve accuracy, an iterative refinement procedure is applied in a small neighborhood of these estimates. The performance of the proposed algorithms was investigated. It is shown that the combined two-stage algorithm produces estimates that are close to the CRLB.

APPENDIX

UNIQUENESS OF THE RELATION BETWEEN THE PHASE AND THE SURFACE TILT AND SLANT ANGLES

In (11) it is shown that the phase function of an harmonic component of the surface texture is transformed by the perspective projection into

$$\Phi(x_i, y_i) = \frac{\frac{x_i}{f} (\tilde{u} \cos \tau - \tilde{v} \cos \sigma \sin \tau) + \frac{y_i}{f} (\tilde{u} \sin \tau + \tilde{v} \cos \sigma \cos \tau)}{\tan \sigma \left(\frac{x_i}{f} \cos \tau + \frac{y_i}{f} \sin \tau \right) + 1} + \varphi \quad (62)$$

measured in the image plane.

Let $\Phi_1(x_i, y_i)$ and $\Phi_2(x_i, y_i)$ be two such phase function with parameters $\tau_1, \sigma_1, \tilde{u}_1, \tilde{v}_1, \varphi_1$ and $\tau_2, \sigma_2, \tilde{u}_2, \tilde{v}_2, \varphi_2$, respectively. To simplify the notations let us rewrite $\Phi_1(x_i, y_i)$ and $\Phi_2(x_i, y_i)$ in the following form:

$$\Phi_1(x_i, y_i) = \frac{\frac{x_i}{f_1} a_1 + \frac{y_i}{f_1} b_1}{\frac{x_i}{f_1} c_1 + \frac{y_i}{f_1} d_1 + 1} + \varphi_1 \quad (63)$$

$$\Phi_2(x_i, y_i) = \frac{\frac{x_i}{f_2} a_2 + \frac{y_i}{f_2} b_2}{\frac{x_i}{f_2} c_2 + \frac{y_i}{f_2} d_2 + 1} + \varphi_2. \quad (64)$$

Theorem 3: Assume $f_1 = f_2, \tilde{u}_1 = \tilde{u}_2$ and $\tilde{v}_1 = \tilde{v}_2$. Then, $\Phi_1(x_i, y_i) = \Phi_2(x_i, y_i)$ for all x_i, y_i if and only if $\tau_1 = \tau_2$ and $\sigma_1 = \sigma_2$.

Proof: Using the notations of (63) and (64) we have to show that $\Phi_1(x_i, y_i) = \Phi_2(x_i, y_i)$ for all x_i, y_i if only if $[a_1, b_1, c_1, d_1, \varphi_1] = [a_2, b_2, c_2, d_2, \varphi_2]$.

It is easy to check that if $[a_1, b_1, c_1, d_1, \varphi_1] = [a_2, b_2, c_2, d_2, \varphi_2]$ then $\Phi_1(x_i, y_i) = \Phi_2(x_i, y_i)$ for all x_i, y_i .



Fig. 10. (Left) Original and (right) orthogonalized aerial images. (Top row) “Stadium.” (Bottom row) “Pier.”

On the other hand, let us assume that $\Phi_1(x_i, y_i) = \Phi_2(x_i, y_i)$ for all x_i, y_i . Hence in particular, $\Phi_1(0, 0) = \Phi_2(0, 0)$. We therefore conclude that $\varphi_1 = \varphi_2$. The assumption $\Phi_1(x_i, y_i) - \Phi_2(x_i, y_i) = 0$ implies that for all x_i, y_i :

$$\begin{aligned} & \left(\frac{x_i}{f}\right)^2 (a_1 c_2 - a_2 c_1) + \left(\frac{y_i}{f}\right)^2 (b_1 d_2 - b_2 d_1) \\ & + \frac{x_i}{f} \frac{y_i}{f} (a_1 d_2 + b_1 c_2 - a_2 d_1 - b_2 c_1) + \frac{x_i}{f} (a_1 - a_2) \\ & + \frac{y_i}{f} (b_1 - b_2) = 0. \end{aligned} \quad (65)$$

This polynomial is identically zero if and only if its coefficients are zero. Hence, we have $[a_1, b_1, c_1, d_1, \varphi_1] = [a_2, b_2, c_2, d_2, \varphi_2]$.

Expressing the equalities $c_1 = c_2$ and $d_1 = d_2$ in terms of the original problem parameters we have

$$\tan \sigma_1 \cos \tau_1 = \tan \sigma_2 \cos \tau_2 \quad (66)$$

$$\tan \sigma_1 \sin \tau_1 = \tan \sigma_2 \sin \tau_2. \quad (67)$$

Hence

$$\cot \tau_1 = \cot \tau_2. \quad (68)$$

Therefore $\tau_2 = \tau_1$ or $\tau_2 = \tau_1 + \pi$. Since $0 < \sigma < \pi/2$, $\tan \sigma_1$ and $\tan \sigma_2$ are positive. Hence, the signs of both $\cos \tau_1$ and $\cos \tau_2$ must be identical. This rules out the possibility that $\tau_2 = \tau_1 + \pi$. Thus $\tau_2 = \tau_1$ and $\sigma_1 = \sigma_2$. ■

ACKNOWLEDGMENT

The authors would like to thank Prof. B. Super for providing them the images for Fig. 8, and to Aerial Images Photography Co. (www.aerialimages-photo.com) for allowing them to use the images in Fig. 10.

REFERENCES

- [1] A. P. Witkin, "Recovering surface shape and orientation from texture," *Artif. Intell.*, vol. 17, pp. 17–45, 1981.
- [2] K. Kanatani, "Detection of surface orientation and motion from texture by a stereological technique," *Artif. Intell.*, vol. 23, pp. 213–237, 1984.
- [3] J. Aloimonos and M. Swain, "Shape from patterns: Regularization," *Int. J. Comput. Vis.*, vol. 2, pp. 171–187, 1988.
- [4] J. V. Stone and S. D. Isard, "Adaptive scale filtering: A general method for obtaining shape from texture," *IEEE Trans. Pattern Anal. Machine Intell.*, vol. 17, pp. 713–719, 1995.
- [5] D. Blostein and N. Ahuja, "Shape from texture: Integrating texture-element extraction and surface estimation," *IEEE Trans. Pattern Anal. Machine Intell.*, vol. 11, pp. 1233–1251, 1989.
- [6] K. Kanatani and T. C. Chou, "Shape from texture: General principle," *Artif. Intell.*, vol. 38, pp. 1–48, 1989.
- [7] L. Y. Jau and R. T. Chin, "Shape from texture using the wigner distribution," *Comput. Vis., Graph. Image Process.*, vol. 52, pp. 248–163, 1990.
- [8] L. G. Brown and H. Shvaytser, "Surface orientation from projective foreshortening of isotropic texture autocorrelation," *IEEE Trans. Pattern Anal. Machine Intell.*, vol. 12, pp. 584–588, 1990.
- [9] M. A. S. Patel and F. Cohen, "Local surface shape estimation of 3-D textured surfaces using Gaussian Markov random fields and stereo windows," *IEEE Trans. Pattern Anal. Machine Intell.*, vol. 15, pp. 1091–1098, 1993.
- [10] H. K. Hong, Y. C. Myung, and J. S. Choi, "3-D analysis of projective textures using structural approaches," *Pattern Recognit.*, vol. 32, pp. 357–364, 1999.
- [11] D. H. Ballard and C. M. Brown, *Computer Vision*. Englewood Cliffs, NJ: Prentice-Hall, 1982.
- [12] R. Stoica, J. Zerubia, and J. M. Francos, "The two-dimensional wold decomposition for segmentation and indexing in image libraries," *Int. Conf. Acoustics, Speech, Signal Processing*, 1998.
- [13] J. Garding, "Shape from texture for smooth curved surfaces," in *Proc. Eur. Conf. Computer Vision*, Italy, 1992, pp. 630–638.
- [14] B. Super and A. C. Bovik, "Planar surface orientation from texture spatial frequencies," *Pattern Recognit.*, vol. 28, pp. 729–743, 1995.
- [15] S. Mann and S. Haykin, "Time frequency perspectives: The chirplet transform," in *Proc. Int. Conf. Acoustics, Speech, Signal Processing*, vol. 3, San Francisco, CA, 1992, pp. 417–420.
- [16] H. Permuter and J. M. Francos, "A parametric approach for estimating the orientation of planar surfaces," *IEEE Int. Conf. Image Processing*, 1998.
- [17] W. L. Hwang, C. S. Lu, and P. C. Chung, "Shape from texture: Estimation of planar surface orientation through the ridge surfaces of continuous wavelet transform," *IEEE Trans. Image Processing*, vol. 7, pp. 773–780, 1998.
- [18] J. M. Francos and B. Friedlander, "Two-dimensional polynomial phase signals: Parameter estimation and bounds," *Multidimen. Syst. Signal Process.*, vol. 9, pp. 173–205, 1998.
- [19] B. Friedlander and J. M. Francos, "An estimation algorithm for 2-D polynomial phase signals," *IEEE Trans. Image Processing*, vol. 5, pp. 1084–1087, 1996.
- [20] P. R. Read and S. Treitel, "The stabilization of two-dimensional recursive filters via the discrete Hilbert transform," *IEEE Trans. Geosci. Electron.*, vol. GE-11, pp. 153–207, 1973.

- [21] Y. M. Zhu, F. Peyrin, and R. Goutte, "The use of a two-dimensional Hilbert transform for Wigner analysis of two-dimensional real signals," *Signal Process.*, vol. 19, pp. 205–220, 1990.
- [22] B. Picinbono, "On instantaneous amplitude and phase signal," *IEEE Trans. Signal Processing*, vol. 45, pp. 552–560, 1997.
- [23] J. M. Francos, A. Z. Meiri, and B. Porat, "A unified texture model based on a 2-D Wold like decomposition," *IEEE Trans. Signal Processing*, vol. 41, pp. 2665–2678, 1993.
- [24] B. Friedlander and J. M. Francos, "Model based 2-D phase unwrapping," *IEEE Trans. Signal Processing*, vol. 45, pp. 2999–3007, 1997.
- [25] P. Maragos, J. F. Kaiser, and T. F. Quatieri, "On amplitude and frequency demodulation using energy operators," *IEEE Trans. Signal Processing*, vol. 41, pp. 1532–1549, 1993.
- [26] A. C. Bovik, N. Gopal, T. Emmoth, and A. Restrepo, "Localized measurements of emergent image frequencies by Gabor wavelets," *IEEE Trans. Inform. Theory*, vol. 38, pp. 691–712, 1992.
- [27] J. M. Francos and B. Friedlander, "Optimal parameter selection in the phase differencing algorithm for 2-D phase estimation and unwrapping," *IEEE Trans. Signal Processing*, vol. 47, pp. 273–279, 1999.
- [28] B. Porat, *Digital Processing of Random Signals*. Englewood Cliffs, NJ: Prentice-Hall, 1994.
- [29] H. Permuter and J. M. Francos, "Estimating the orientation of planar surfaces: Algorithms and bounds," *IEEE Trans. Inform. Theory*, vol. 46, pp. 1908–1920, 2000.



Joseph M. Francos (M'90–SM'97) was born in Tel-Aviv, Israel, in 1959. He received the B.Sc. degree in computer engineering in 1982, and the D.Sc. degree in electrical engineering in 1990, both from the Technion—Israel Institute of Technology, Haifa.

From 1982 to 1987, he was with the Signal Corps. Research Laboratories, Israeli Defense Forces. From 1991 to 1992, he was with the Department of Electrical Computer and Systems Engineering, Rensselaer Polytechnic Institute, Troy, NY, as a Visiting Assistant Professor. During 1993, he was with Signal Processing Technology, Palo Alto, CA. In 1993, he joined the Department of Electrical and Computer Engineering, Ben-Gurion University, Beer-Sheva, Israel, where he is now an Associate Professor. He also held visiting positions at the Massachusetts Institute of Technology Media Laboratory, Cambridge, at the Electrical and Computer Engineering Department, University of California, Davis, and at the Electrical Engineering and Computer Science Department, University of Illinois, Chicago. His current research interests are in parametric modeling and estimation of 2-D random fields, random fields theory, parametric modeling and estimation of nonstationary signals, image modeling and indexing, and texture analysis and synthesis.

Dr. Francos is currently serving as an Associate Editor for the IEEE TRANSACTIONS ON SIGNAL PROCESSING.



Haim H. Permuter was born in Romania in 1975. He received the B.Sc. degree (summa cum laude) in electrical and computer engineering in 1997 from the Ben-Gurion University, Beer-Sheva, Israel, where he is currently a graduate student.

Since 1997, he has been with an R&D unit of the Israeli Defense Forces. His current research interests are in signal processing and pattern recognition.

Mr. Permuter is a recipient of the Eshkol Fellowship (1996–1997).